Three-Dimension Finite Element Analysis of a Helical Motion Induction Motor

J. H. Alwash[1] and L. J. Qaseer[2]

Department of Electrical Engineering
Uuniversity of Baghdad, Jaderia, Baghdad, Iraq
jalwash@yahoo.com

General & Theoretical Electrical Engineering Department
University of Duisburg-Essen
Bismarckstrasse 81, 47057, Duisburg, Germany
laythqaseer@yahoo.com

Abstract **-** The paper presents a three-dimensional finite element analysis applicable to all forms of sheet rotor, cylindrical, linear induction motor, as well as, helical motion induction motor. The analysis accounts for longitudinal and transverse end effects, skin depth and finite sheet thickness; furthermore, there is practically no restriction on the shape of magnetic circuit that can be considered. It yields detailed space profile of the state variables. The winding arrangement may include multi-polar system circumferentially and axially. The excitation produced by such winding is a helically traveling wave. The formulation results in a set of linear equations which are solved by point relaxation method. The solution algorithm employs power mismatch in the machine to indicate accuracy. The theory is supported by experimental results.

Index Terms **-** AC machines, finite element methods, induction motors, numerical analysis.

I. INTRODUCTION

The two-degree of mechanical freedom actuator capable of linear, rotation, or helical motion would be a desirable asset to the fields of machine tools and robotics. The magnetic circuits suggested for such a machine use laminations transverse to the direction of motion.

In a previous paper [1], a tubular motor with a double helical winding was presented using a multi–layer mathematical model for the analysis. Mendrela and Turowski [2], Fleszar and Mendrela [3], and Mendrela and Gierczak [4] reported analysis of helical motion induction motor (HMIM) using the Fourier series method which takes into account the end effects.

Cathey [5] and Rabiee and Cathey [6, 7] had presented a helical motion induction motor and a procedure was developed for the determination of the equivalent circuit parameters even though the magnetizing inductance is small for a typical secondary of conducting sleeve design. It was shown that under appropriate definition of slip the Steinmetz equivalent circuit of an induction motor can be applied to this two degree of freedom machine.

In a later paper, Alwash, Mohssen and Abdi [8] presented a multi–layer theory analysis of HMIM with any number of axial and circumferential poles and that the method retains the true cylindrical topology of the machine under consideration.

The object of this paper is to present a three–dimensional (3-D) finite element analysis of HMIM, since the helical winding topology is not axisymmetric and, hence, cannot be analyzed using a two-dimensional finite element method. The formulation is derived using a variational approach, the problem of induction in moving media is being treated by the extension of a

previous finite element solution, of electromagnetic field problems [9, 10]. The solution, which appears to behave well numerically, employs a convergence test devised from power balance considerations in the machine.

II. THEORETICAL ANALYSIS

The general outline of the model is shown in Fig. 1. *r,* θ and *z* are cylindrical coordinates. The quantities p_z, V_θ and V_z represent axial pole pitch, circumferential rotor velocity and axial rotor velocity respectively. The rotor conducting sheet moves in both axial (z) and circumferential (θ) directions.

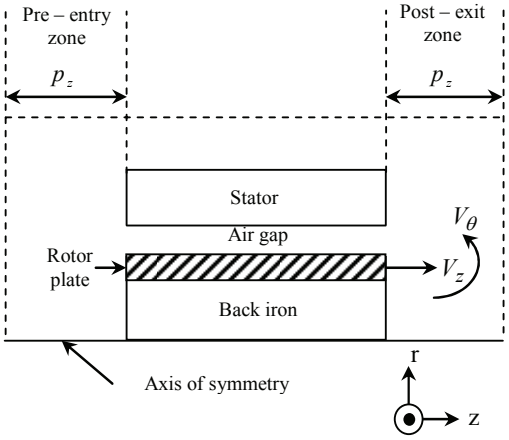

Fig. 1. General outline of the model.

The solution, where ω represents the angular frequency, is based on the following assumptions:

1. The stator current is known and has two cylindrical components, namely J_θ and J_z.

2. All fields vary with time as $\exp(j\omega t)$ and decay to zero at sufficiently far distances from the machine axis.

3. Displacement currents and laminated iron conductivity are not considered.

The above assumptions are quite common in machine analysis. It is noted that they impose no restriction on the topology of the machine in the rz – plane, thus allowing treatment of all practical forms of sheet rotor cylindrical linear induction motors.

A. Stator current density

It is assumed that the winding produces perfect sinusoidal traveling wave. The line current density J_o may be represented as [8]:

$$J_o = J_s \exp j(\omega t - kz + n\theta), \tag{1}$$

where *k* and *n* represent the wave length factor defined below and number of circumferential pole pairs in helical system respectively. The stator line current density J_s is defined as:

$$J_s = J_m \exp(j\phi),$$

where

$$\phi = \tan^{-1}\frac{n}{k \cdot r_g}, \tag{2}$$

$$k = \frac{\pi \cdot \cos(\phi)}{p}, \tag{3}$$

with J_m, ϕ, r_g and *p* representing amplitude of line current density, helicoid angle, inner stator radius and normal pole pitch respectively.

B. Governing equations

For a 3-D analysis, Maxwell's equations require that the vector potential $A(r,\theta,z)$ satisfies [9], such that

$$\nabla \times \left(\frac{1}{\mu}\nabla \times \overline{A}\right) = \overline{J}, \tag{4}$$

where $\overline{A}$ and $\overline{J}$ represent the three dimensional magnetic vector potential and the current density vector respectively. According to assumption (1), the above equation leads to two Euler equations in cylindrical coordinates (or three equations in Cartesian coordinates). Depending on the position, the current density takes the following values:

Stator winding region

$$\overline{J} = \overline{J}_0. \tag{5a}$$

Non conducting region

$$\overline{J} = \overline{0}. \tag{5b}$$

Rotor conducting sheet

$$\overline{J} = -j\omega\sigma\overline{A} + \sigma\left(\overline{V} \times \overline{B}\right), \tag{5c}$$

where σ, $\overline{V}$ and $\overline{B}$ represent rotor conductivity, three dimensional velocity vector and magnetic flux density vector. Equations (4) and (5), and the

zero potential conditions assumed at the outermost boundaries, as well as machine axis, specify the problem in differential form and should yield a unique solution for the magnetic vector potential.

Now, the solution of equation (4) is known to minimize the energy functional χ [12]

$$\chi = \iiint_{\Omega} \left\{ \frac{1}{2\mu}\left(B_r^2 + B_\theta^2 + B_z^2\right) - \overline{A}\cdot\overline{J} \right\} r dr d\theta dz \,, \quad (6)$$

where Ω denotes the entire domain considered in the analysis; this may be simply verified by applying Euler's theorem of variational calculus to show that (4) is the Euler equation corresponding to χ as defined in (6).

C. Performance calculations

Once the potential distribution in the system is known, it is possible to compute all quantities of interest. These include the rotor induced current density, flux density components, propulsion force, the rotational torque, the power supplied, the air gap power, the rotor ohmic losses, stator voltage, input power factor and the efficiency [9]. The performance parameters mentioned above require derivatives and integrals involving the magnetic vector potential. Only force calculations will be be considered here.

1) The propulsion force:

The calculation of propulsion force, in particular, requires some consideration, as there are three methods.

The first method is the Maxwell stress method which states that the time average axial force F_z on a volume element can be calculated by integrating the electromagnetic stress over its surface, with H_r, H_θ, and H_z being the radial, circumferential and axial components of magnetic field strength vector and μ_0 is the permeability of free space

$$F_z^e = \frac{1}{2}\mathrm{Re}\left\{ \iint_s \mu_o H_r H_z^* ds \right\}. \quad (7)$$

Choosing a volume which consists of a cylinder of radius R bounded at its ends by the outer boundaries, it is possible to write:

$$F_z^e = \frac{R(\Delta\theta)}{2}\mu_o \int_{z_{\min}}^{z_{\max}} \mathrm{Re}\left\{H_r H_z^*\right\} dz \,. \quad (8)$$

This requires finding the contribution to the force from all elements that span the radius R where the cylinder encloses the rotor. For a typical element shown in Fig. 2, the time average value of the force on the rotor conductor is given by:

$$F_z = \frac{R}{2\mu_o}\left[z_{\max} - z_{\min} \right] . \sum_e \mathrm{Re}\left\{ B_r^e B_z^{*e} \right\} (\Delta\theta) . \quad (9)$$

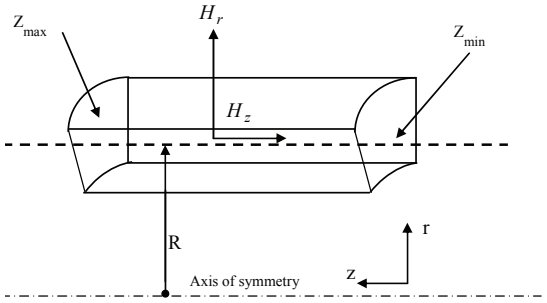

Fig. 2. Typical element for the calculation of propulsion force.

The second method is $\overline{J}\times\overline{B}$ on a stator winding region where the time average propulsion force per unit volume is obtained by taking the z – component in (9), therefore

$$f_z^e = -\frac{1}{2}\mathrm{Re}\left\{ J_\theta^e B_r^{*e} \right\} \quad \mathrm{N/}m^3 \,.$$

Hence, the time average propulsion force on an element can be written as:

$$F_z^e = -\frac{1}{2}\mathrm{Re}\left\{ \iiint_e J_\theta^e B_r^{*e}\, r dr d\theta dz \right\},$$

and the total time average propulsion force on the rotor conductor now becomes:

$$F_z = -\frac{1}{2}\sum_e \mathrm{Re}\left\{ J_\theta^e B_r^{*e} \right\} \Delta v \quad \mathrm{N}, \quad (10)$$

where $\Delta v = r_c \Delta r \Delta\theta \Delta z$.

The summation is carried out over all elements in the stator winding region.

The third method is $\overline{J}\times\overline{B}$ on rotor region

where the calculation of the force by $\left(\overline{J}\times\overline{B}\right)$ on an eddy current region is similar to that on a current source region. The only difference being that the induced current density is used rather than the specified stator current density. For an iron cored rotor rotary-linear motor, this method can lead to errors as it neglects the forces which act directly on the iron.

2) The rotational force:

The time average rotational force per unit volume is given by

$$f_\theta^e = \frac{1}{2}\mathrm{Re}\left\{J_z^e B_r^{*e}\right\} \quad \mathrm{N}/m^3$$

$$\text{or} \quad F_\theta^e = \frac{1}{2}\mathrm{Re}\left\{\iiint_e J_z^e B_r^{*e}\, dv\right\} \quad \mathrm{N},$$

and the total time average rotational force on the rotor conductor now becomes

$$F_\theta = \sum_e F_\theta^e , \qquad (11)$$

where the summation is carried out over all elements in stator winding region. The circumferential (rotational) torque can be obtained simply by multiplying the circumferential force by the radius of the stator over which the integration is carried out.

3) The radial force:

The radial component of the Lorentz force per unit volume on each element in a conductor is given by

$$f_r^e = \frac{1}{2}\mathrm{Re}\left\{J_\theta^e B_z^{*e} - J_z^e B_\theta^{*e}\right\} \quad \mathrm{N}/m^3 .$$

Due to rotor circular symmetry of RLIM, the rotor experiences no radial force, therefore

$$F_r = \sum_e f_r^e\, dv = 0 .$$

III. EXPERIMENTAL MACHINE

To verify the theoretical results obtained through the computation, laboratory measurements were made on two experimental machines. The first model A was constructed by Cathey and Rabiee in [6,7]. It was an iron cored stator iron cored rotor machine. Extensive analysis for this model is made with standstill and variable speed analysis for the state variables.

Model B was constructed by Alwash, Mohssen and Abdi [8] at the University of Baghdad. The stator of this machine contains no iron and hence is considered as an open magnetic circuit. The model was tested with variable frequency under standstill conditions.

Table 1. Machine parameters for Model A.

Parameter	Value
Stator length, m	182.8
Phases	3
Circumferential poles	2
Axial poles	2
Slots per pole per phase	2
Slots per pole	6
Slots, axial & circumferential	12, 12
Normal coil width, mm	7.18
Normal slot pitch, mm	10.78
Normal pole pitch, mm	64.64
Helicoids angle on primary, degrees	45
Turns per coil	20
Stator phase current, A	15 r.m.s.
Frequency, Hz	60
Circumferential pole pitch at inner stator radius, mm	52.62
Air gap length, mm	2.78
Steel shaft diameter, mm	25.4
Copper sleeve thickness, mm	1.27
Copper rotor conductivity, S/m	4.48×10^7
Shaft relative permeability	750

Table 2. Machine parameters for Model B.

Parameter	Value
Stator length, m	203
Phases	3
Circumferential poles	2
Axial poles	4
Slots per pole per phase	1
Slots per pole	3
Slots, axial & circumferential	12, 6
Normal coil width, mm	7
Normal slot pitch, mm	12
Normal pole pitch, mm	36
Helicoids angle on primary, degrees	36.3
Turns per coil	160
Stator phase current, A	2.3 r.m.s.
Frequency, Hz	50/150/250

Circumferential pole pitch at inner stator radius, mm	50.27
Air gap length, mm	3.5
Steel shaft diameter, mm	25
Copper sleeve thickness, mm	3
Copper rotor conductivity, S/m	3.4×10^7
Shaft relative permeability	56

Tables 1 and 2 show the parameters of models A and B respectively. Table 3 shows the discretization data and CPU time for model A. The computer used was a Pentium 4 (2.4 GHz) PC.

Table 3. Discretization data and CPU time for Model A.

Number of element	325,247
Number of nodes	61,856
Number of edges	409,973
Total CPU time (hours)	1,238

IV. RESULTS

Figures 3 and 4 show respectively the variation of the propulsion force and the circumferential torque with respect to speed for model A at 60 Hz using the finite element method and equivalent circuit model adopted in [6,7] for the sake of comparison. The two methods agree within 5% for the propulsion force. For the circumferential torque, it is clear that the finite element method is closer to measured values than equivalent circuit method while both methods agree with maximum deviation of 5.2 %.

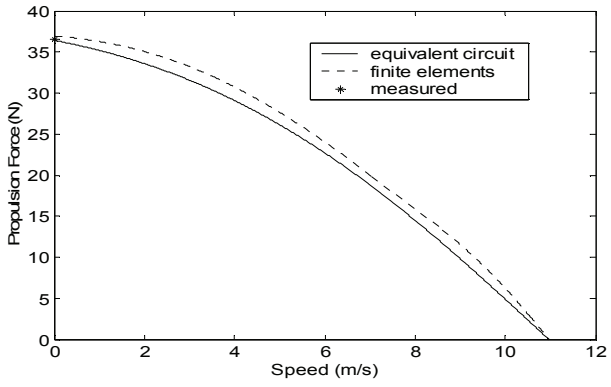

Fig. 3. Propulsion force against speed at 60 Hz for model A.

The power of the finite element method, in addition to its high accuracy compared to the analytical methods lies in its ability to display the effect of finite dimensions (end effects) of the actual machine.

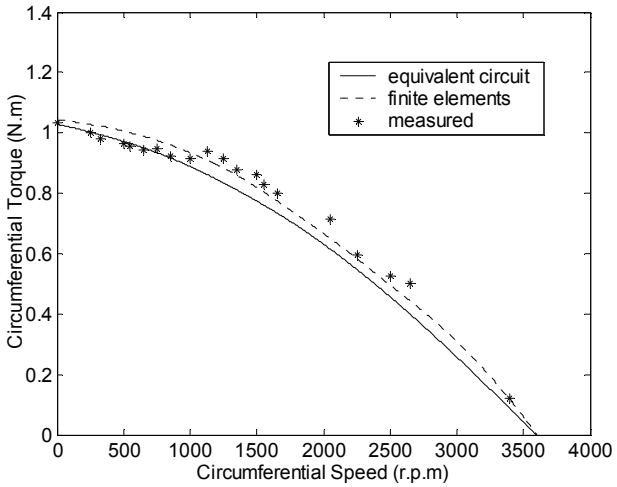

Fig. 4. Circumferential torque against speed at 60 Hz for model A.

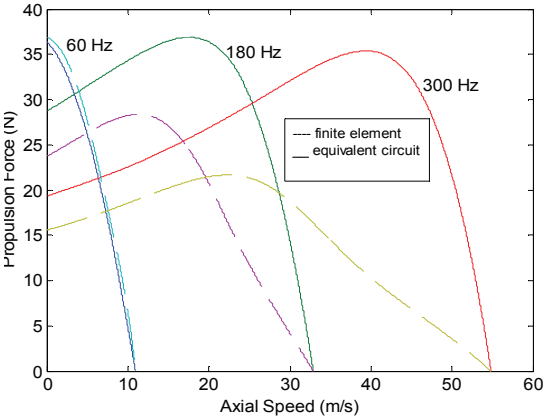

Fig. 5. End effects on propulsion force at different frequencies for model A.

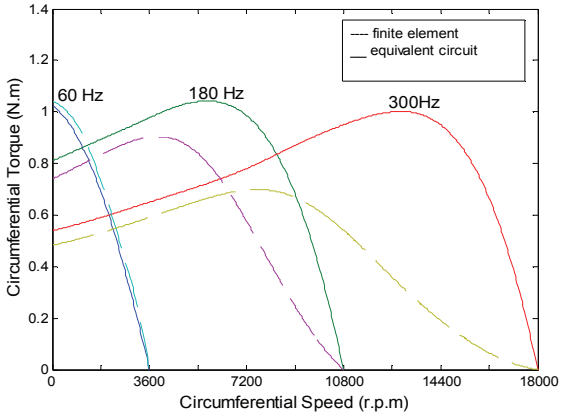

Fig. 6. End effects on circumferential torque at different frequencies for model A.

To validate this, Figs. 5 and 6 show the variation of force and circumferential torque with respect to speed for model A at 60, 180 and 300 Hz using the finite element method and equivalent circuit model. The results show that the end effects are prominent as frequency and speed increase [10] which affect the peak force and torque values when the finite element method is adopted.

Figures 7 to 9 show the flux profile of the model for the three components of flux density at frequency of 60 Hz using three different slips.

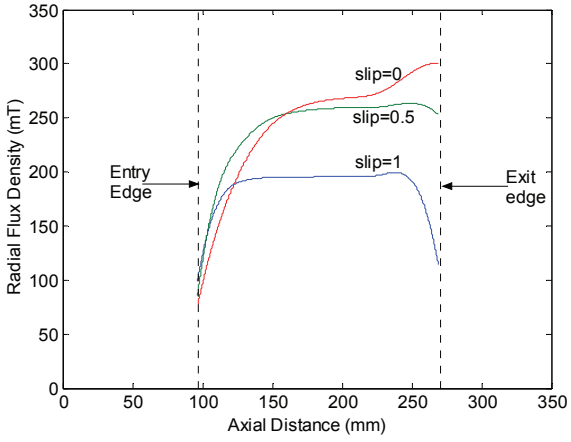

Fig. 7. Radial flux density distribution at 60 Hz for model A.

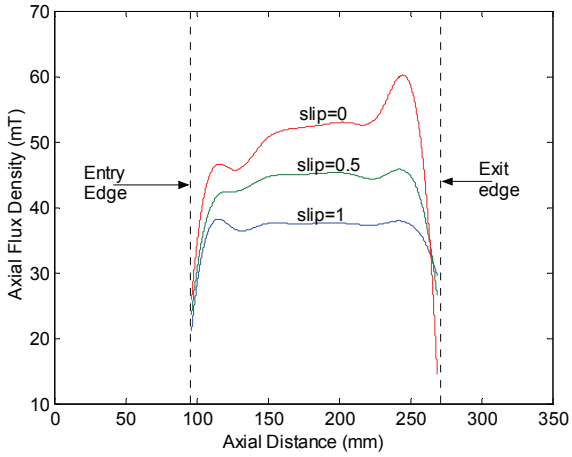

Fig. 8. Axial flux density distribution at 60 Hz for model A.

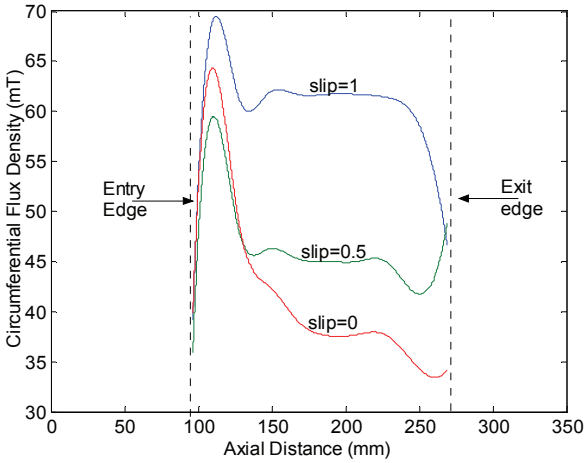

Fig. 9. Circumferential flux density distribution at 60 Hz for model A.

Figures 10 to 13 show the space profile for the rotor current density, air gap power, propulsion force and circumferential torque distributions for model A at standstill and frequencies of 60, 180 and 300 Hz where end effects are prominent and clearly visible.

Figures 14 to 17 show the variation of line terminal voltage, input power, input power factor and efficiency with respect to speed for model A using the finite element method.

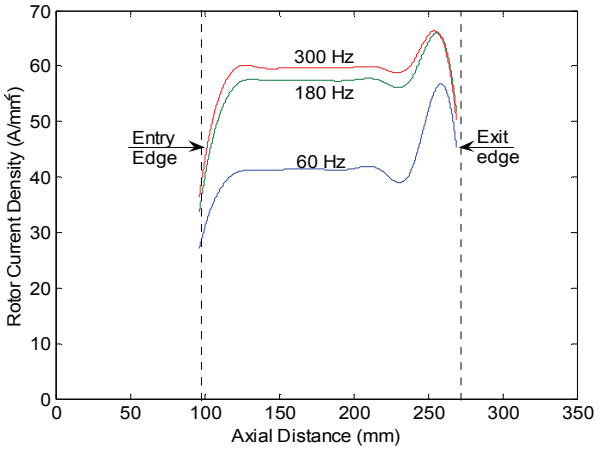

Fig. 10. Rotor current density distribution along axial distance at standstill for model A.

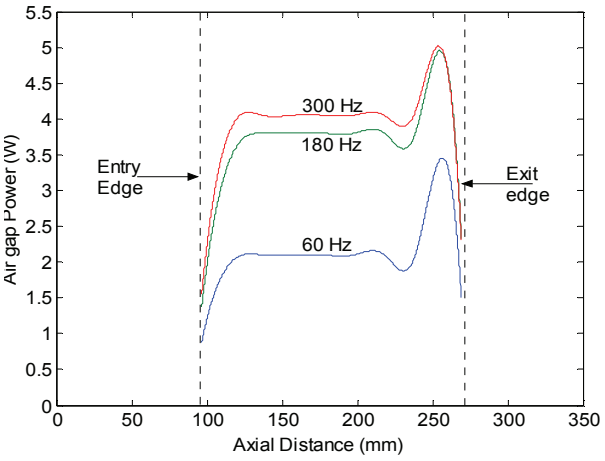

Fig. 11. Air gap power distribution along axial distance at standstill for model A.

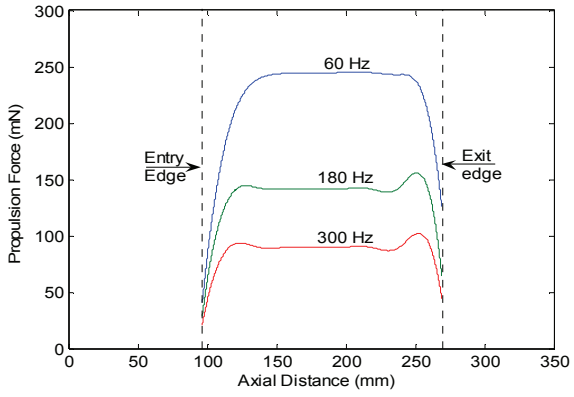

Fig. 12. Propulsion force distribution along axial distance at standstill for model A.

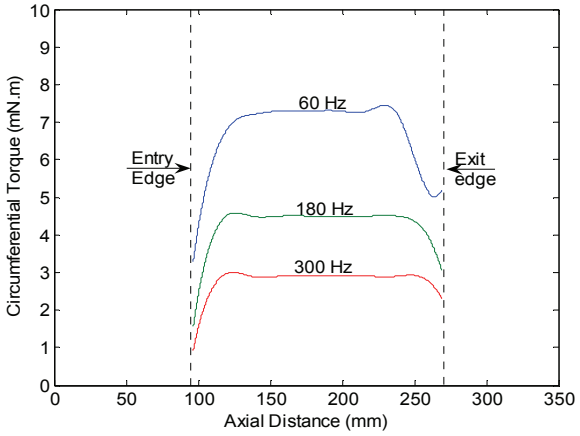

Fig. 13. Circumferential torque distribution along axial distance at standstill for model A.

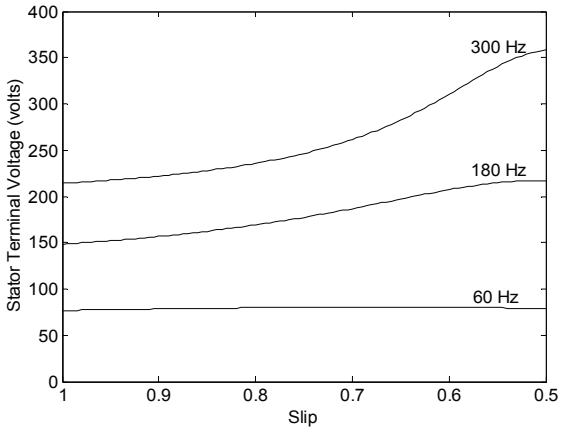

Fig. 14. Stator terminal voltage against speed at different frequencies for model A.

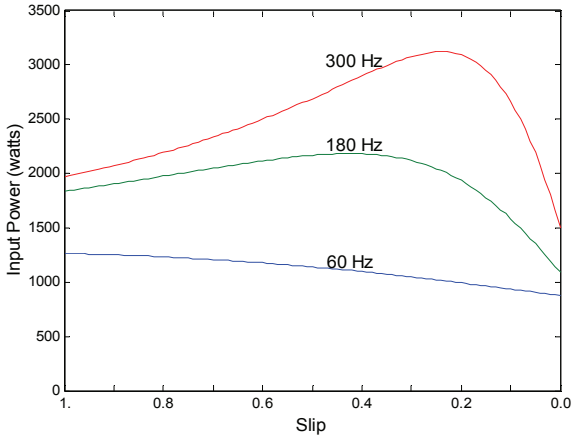

Fig. 15. Input power against speed at different frequencies for model A.

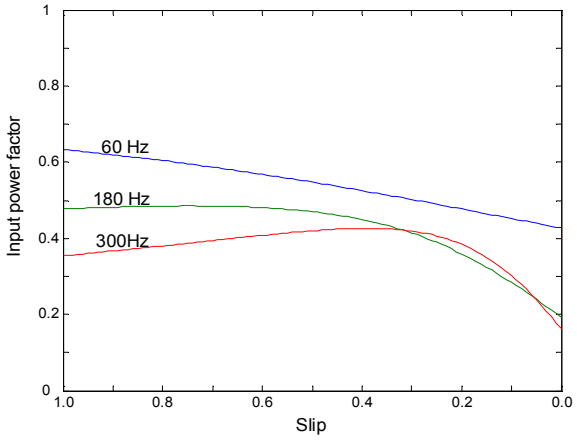

Fig. 16. Input power factor against speed at different frequencies for model A.

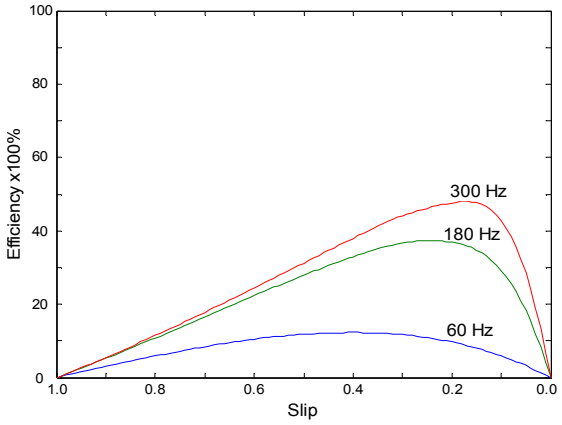

Fig. 17. Efficiency against speed at different frequencies for model A.

Figures 18 and 19 show respectively the variation of propulsion force with frequency for model B using a hollow aluminum rotor and a solid aluminum rotor by introducing the numerical results from the finite element analysis and the computed results of the layer theory approach adopted in [8] against measured values at standstill. Figures 20 and 21 show respectively the variation of the circumferential torque with frequency at standstill for model B using hollow and solid aluminum rotor by introducing finite element results and layer theory results against measured values.

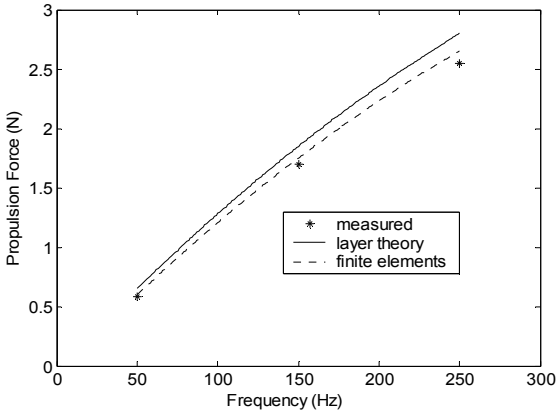

Fig. 18. Propulsion force against frequency for model B with hollow rotor.

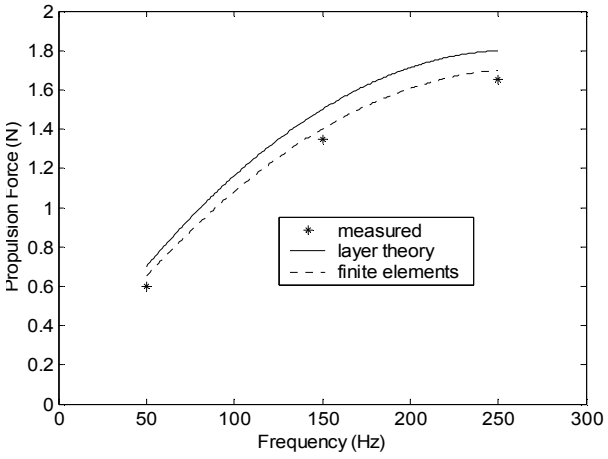

Fig. 19. Propulsion force against frequency for model B with solid rotor.

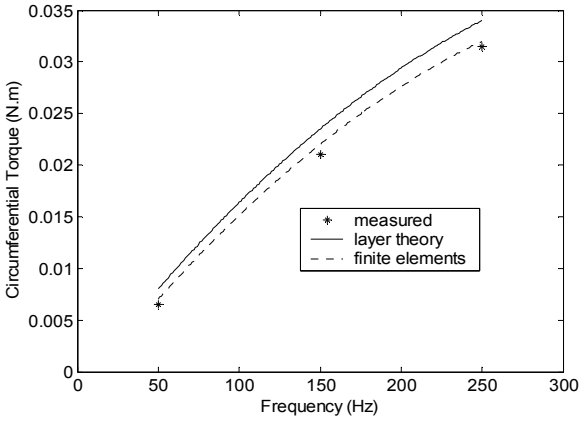

Fig. 20. Circumferential torque against frequency for model B with hollow rotor.

The agreement between layer theory and experimental results lies within a maximum deviation of 7.6% while the agreement between finite element and experimental results lies within a maximum deviation of 3.9%.

It is worth mentioning that in addition to the fact that the finite element method is closer to experimental results than the layer theory approach, the differences between the results of the layer theory approach and finite element computations increase with increasing frequency due to longitudinal end effects, which becomes more effective at higher frequencies.

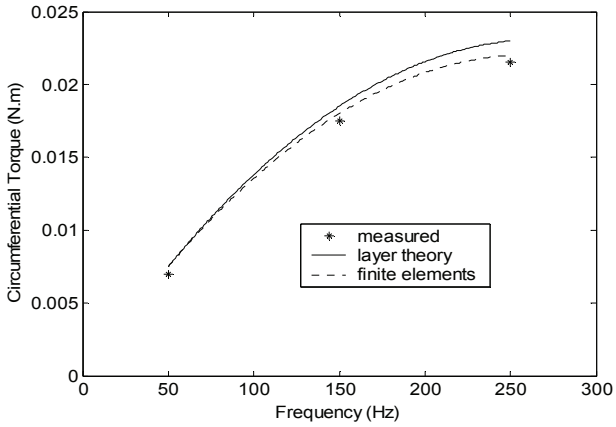

Fig. 21. Circumferential torque against frequency for model B with solid rotor.

V. CONCLUSION

The 3-D finite element method has been used for the analysis of helical motion induction motors. The methodology presented is quite general as it lends itself to the analysis of tubular linear induction motors and cylindrical induction heating systems. It is shown for the models considered that longitudinal end effects are most effective at higher frequencies and speeds. An important conclusion inferred from our study is that end effects must play an important part in these machines. The 3 – D finite element method has been shown to be eminently suited to the analysis of helical induction machines. The results, displayed and discussed in the previous section, show clearly that the finite element results agree well with the experimental ones more than any other closed form technique. This may be considered as a fair justification of the analysis method proposed in this paper.

ACKNOWLEDGMENT

L. J. Qaseer is deeply indebted to Daniel Erni, his host and co-worker at the University of Duisburg-Essen for advice and encouragement.

REFERENCES

[1] J. F. Eastham and J. H. Alwash, "Transverse flux tubular motors," *Proc. IEE*., vol. 112, no. 12, pp. 1709-1718, Dec. 1972.

[2] E. A. Mendrela and J. Turowski, "Rotary-linear induction motor," *IEEE winter power meeting*, New York, no. A78 091-1, 1978,

[3] J. Fleszer and E. A. Mendrela, "Twin–armature rotary–linear induction motor," *Proc. IEE* pt. B, vol. 130, no. 3, pp. 186–192, May 1983.

[4] E. A. Mendrela and E. Geirczak, "Double–winding rotary–linear induction motors," *IEEE Trans. Energy Convers.*, vol. EC–2, no. 1, pp. 48–54, March 1987.

[5] J. J. Cathey, "Helical motion induction motor," *Proc. IEE* pt. B, vol. 132, no. 2, pp. 112–114, March 1985.

[6] M. Rabiee and J. J. Cathey, "Verification of a field theory analysis applied to a helical motion induction motors," *IEEE Trans. Magn.*, vol. 24, no. 4, pp. 127–138, July 1988.

[7] J. J. Cathey and M. Rabiee, "Verification of an equivalent circuit model for a helical motion induction motor", *IEEE Trans. Energy Convers.*, vol. 3, no. 3, pp. 660–666, Sept. 1988.

[8] J. H. Alwash, A. D. Mohssen and A. S. Abdi, "Helical motion tubular induction motor," *IEEE Trans. Energy Convers.,* vol. 18, no. 3, pp. 362– 396, Sept. 2003.

[9] T. Yamaguchi, Y. Kawase, M. Yoshida, Y. Saito and Y. Ohdachi, "3 – D finite element analysis of a linear induction motor," *IEEE, Trans. Magn*., vol. 37, no. 5, pp. 3668–3671, Sept. 2001.

[10] M. A. Al–Maayouf, "*Study of a Linear Induction Motor Using Alternative Models,*" Ph. D thesis, City University, London, U. K., 1981.

J. H. H. Alwash was born in Babylon, Iraq, on March 7, 1945. He graduated from University College London in 1967 and obtained his Ph.D. degree from London University in 1972 as an internal student of both Kings College & Imperia college of Science & Technology. He is now a Professor of Electrical Engineering Department, University of Baghdad. His special fields of interest included induction machines (rotary, flat linear and tubular linear types) and induction heating.

L. J. B. Qaseer was born in Baghdad, Iraq, on October 14, 1957. He received his B.Sc., M. Sc. and Ph.D. degrees from the University of Baghdad in 1979, 1993 and 2004 respectively, all in electrical engineering. In 2005, he was with the Mechatronic Engineering Department at the University of Baghdad. Dr. Qaseer is currently with the General & Theoretical Electrical Engineering Department of the University of Duisburg-Essen, Duisburg, Germany. His special fields of interest include rotary, linear, tubular linear and helical motion induction motors, as well as, induction heating.